Acoustic Assessment of an MD530F Helicopter in Maneuvering Flight

Colin M. Stutz
Aerospace Research Engineer
NASA Langley Research Center
Hampton, VA, USA

James H. Stephenson
Aviation Acoustics SME
U.S. Army Combat Capabilities Development Command
Aviation & Missile Center Hampton, VA, USA

Kyle A. Pascioni
Aerospace Research Engineer
NASA Langley Research Center
Hampton, VA, USA

Mary L. Houston
Aerospace Research Engineer
NASA Langley Research Center
Hampton, VA, USA

ABSTRACT

A joint acoustic flight test was conducted by NASA Langley Research Center and the U.S. Army Combat Capabilities Development Command Aviation & Missile Center, with the goal of investigating new methods for acoustic data collection. The impetus for the effort is the anticipated growth of Urban Air Mobility and Future Vertical Lift vehicles. Many of these vehicles are expected to have distributed propulsion systems that may result in unsteady vehicle state conditions even during steady flight. This work examines the acoustic measurements collected during purposefully unsteady maneuvers performed by an MD530F helicopter. A snapshot microphone array design was deployed for this test to capture the acoustic signature on the ground from the helicopter under maneuver conditions. An analysis of the acoustic emissions indicated the presence of blade-vortex interactions, not only during the rolls towards the advancing side of the main rotor, but also rolls towards the retreating side and during pitch-up maneuvers. The strength of the interaction noise was found to be strongly dependent on the acceleration of the vehicle.

INTRODUCTION

The NASA Langley Research Center and the U.S. Army Combat Capabilities Development Command Aviation & Missile Center conducted a joint acoustic flight test in July 2024. The test was designed to investigate new research methods for the characterization of rotorcraft acoustic emissions. An MD530F helicopter was used as the test vehicle; however, future tests are anticipated to include Urban Air Mobility (UAM) and Future Vertical Lift (FVL) vehicles. UAM and FVL vehicles are often designed with multiple smaller independently controlled propulsors as opposed to the traditional designs of helicopters. This can lead to vehicle designs that exhibit time-varying propulsor operating states, even in steady flight, as well as interactional aeroacoustic noise sources (Refs. 1, 2). There have been efforts to study these types of vehicles computationally (Refs. 3, 4), but full-scale experimental data are scarce and, therefore, will likely be the focus of future tests. These considerations led to the inclusion of unsteady maneuvers in the test campaign as a way to investigate measurement techniques to capture the acoustic emissions from unsteady flight. Past studies including transient maneuvers highlight the difficulties in capturing acoustic emissions from unsteady conditions (Refs. 5–8), reinforcing the idea that transient maneuvers could serve as sufficient stand-ins for UAM- and FVL-relevant unsteady flight conditions. The pilot was instructed to attempt to fly each maneuver as a single-input condition even if that results in several changes in vehicle state. For instance, speed and pitch are not adjusted during a roll maneuver, which would be required to maintain forward speed and altitude. This allowed the vehicle to lose altitude during the roll. Note that one condition was specified as a combined cyclic and collective pitch up, which inherently required two inputs, however, the intent was still to isolate the desired control input.

FLIGHT TEST DESCRIPTION

This flight test was conducted by the NASA/Army Comprehensive Rotorcraft Acoustic Flight Test Team at the Sierra Army Depot's Amedee Army Airfield from 8 July to 28 July 2024. During this period, data were collected on six flight days totaling 21 hours of flight testing. Data will be referred to based on the 6-digit combined NASA run number, *FFFRRR*, where *FFF* is the flight number (Julian date, e.g., 15 July 2024 is 197), and RRR is the run number. A complete overview of the test, including details on the flight vehicle, is provided in Ref. 9. The vehicle used for this test was a highly instrumented MD530F helicopter, which has an empty weight

The Vertical Flight Society's 81st Annual Forum and Technology Display, Virginia Beach, VA, May 20-22, 2025.

of 782 kg, a counter-clockwise-rotating 5-bladed main rotor with a diameter of 8.34 m, and a main rotor blade passage frequency (BPF) of 39.75 Hz.

A variety of weather measurement instrumentation was deployed throughout the test, details of which can also be found in Ref. 9. Multiple microphone arrays were deployed throughout the test campaign; however, only the snapshot array was considered during the testing of maneuvering flight. The snapshot array was designed to provide uniform hemispherical coverage directly under the vehicle at an altitude of 61 m (200 ft) and used 79 microphones. The microphone positions were measured with a differential GPS survey system to capture any deviations between array design and deployment. The center of the array was used as the origin point of the coordinate system, with positive X being along the flight path, positive Y to the port side (left) of the vehicle, and positive Z pointing up. The design of the snapshot array is shown in Figure 1 in both Cartesian coordinates (as deployed) and in a Lambert projection. The Lambert projection is oriented such that it covers the entire lower hemisphere around the vehicle, where 0° azimuth is the tail, 180° azimuth is the nose, 90° and 270° azimuth are starboard and port, respectively, 0° elevation is the main rotor plane, and -90° elevation is directly below the vehicle. Typically, when forming a noise hemisphere, the rotor plane may be assumed to correspond with the global horizon plane. However, due to the severity of the maneuvers, some microphones during the pitch and roll motions become positioned above the rotor plane, at which point elevation angles are positive such that 0° is still the main rotor plane and 90° is directly above the vehicle. Lastly, five microphones have been given unique markers in the figures of this paper to aid in comparison and understanding of the layout under various conditions. Details on the design and data processing for the snapshot array are described in Ref. 10.

Acoustic data for the snapshot array were collected using NASA's Wireless Acoustic Measurement System version II (WAMS II), which are remotely controlled systems with local data storage. Each WAMS II unit includes a microphone, ground board, GPS receiver, and radio antenna. The GPS receiver provides UTC timestamps for the recorded data, allowing the synchronization of the collected acoustic, vehicle, and weather data. Seventy-five of the units utilized GRAS 67AX microphones (ground-board embedded) and the 4 innermost units used B&K 4964 microphones (inverted 6.35 mm above ground boards). All microphones were offset from the center of the ground boards to mitigate edge effects, and oriented such that the microphone was at the far edge of the board relative to the array center. A deployed WAMS II unit is depicted in Ref. 9. The units are triggered such that every deployed microphone starts and stops recording simultaneously. For this deployment, the microphones were sampled at 50 kHz with 24-bit resolution.

Multiple flight conditions were used for this test, including level flights, steady climbs, steady descents, hovers, and previously mentioned unsteady maneuvers. The design of the test points for the snapshot array was part of an investigation on the use of Design of Experiments (DOE) for flight tests. The DOE schemes are summarized in Ref. 9 and described in detail in Ref. 11. The unsteady-maneuver flight test conditions, which will be the focus of this work, are summarized in Table 1. The final entry in the table is the steady, level flight condition at the same flight speed and altitude as the maneuver entry conditions, and will be used as the reference condition throughout this work. Each condition was chosen to represent a single-input maneuver from the pilot and flown such that the maneuver began approximately over the center of the array.

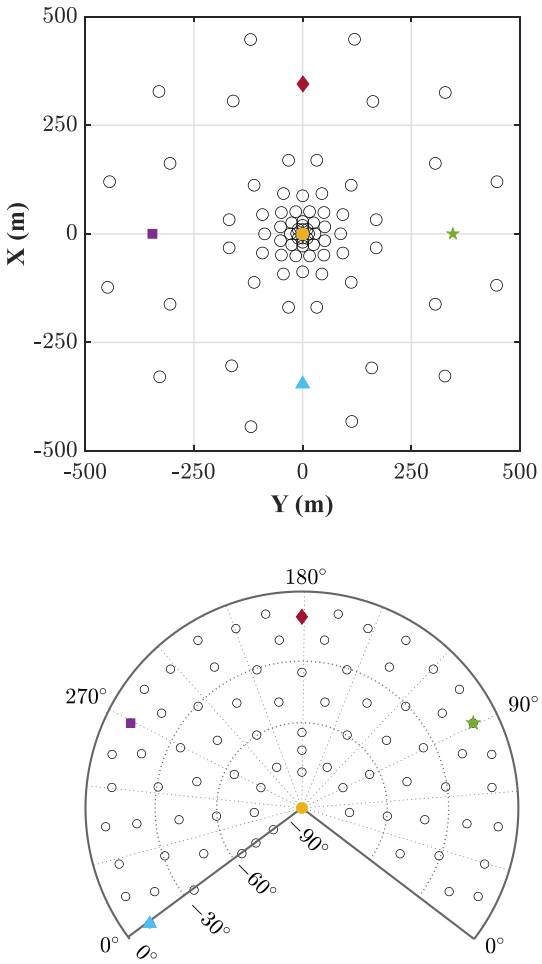

Figure 1: Designed layout of snapshot array in Cartesian coordinates (top) and a Lambert hemisphere projection (bottom).

Information on the vehicle's positional and inertial state is critical for contextualizing the collected acoustic data. This information was collected continuously for each flight day using NASA's Aircraft Navigation and Tracking System (ANTS). The data collected by ANTS is described in Ref. 9, and more detailed descriptions of the ANTS system are included in Refs. 12 and 13. The vehicle was also outfitted with additional instrumentation that recorded information such as

Table 1: Maneuver Conditions

Condition Code	Description	Entry Speed (kts)	Entry Altitude (m AGL)	NASA Run Numbers
M1	Cyclic roll right, fast	75	61	206542, 206544
M2	Cyclic roll left, fast	75	61	206543, 206545
M3	Cyclic roll right, slow	75	61	206546, 206548
M4	Cyclic roll left, slow	75	61	206547 206549
M5	Pitch up, cyclic	75	61	206550, 206553
M6	Pitch up, collective	75	61	206551, 206554
M7	Pitch up, cyclic and collective	75	61	206552, 206555
L3	Steady, level flight	75	61	206501, 206510

the vehicle stick positions. The additional instrumentation is documented in Ref. 9.

DATA REDUCTION

The following section documents the specific processes applied to the data used in this work. A more general description of the data reduction process for this test is provided in Ref. 9.

Vehicle State Data

Vehicle state data were parsed on a per-run basis based on the recorded Coordinated Universal Time (UTC) and the beginning and end times of recorded acoustic data. All times shown in this work have been adjusted such that t = 0 s is the time that the vehicle crossed over the center of the array. Position, velocity, and acceleration data were adjusted to match the coordinate system described previously. Acceleration, a, will be reported in this work in units of g's. Pitch (α), roll (ϕ), and heading (H) angles were also recorded. Flight path angle (γ) and rates of change for pitch (dα/dt) and roll (dϕ/dt) angles were calculated for each flight. An effective flight path angle (γ_{eff}) was also calculated, using the definition from Ref. 14 and provided in Equations 1-3. Effective flight path angle provides an estimate of the flight path angle with respect to the rotor tip-path-plane during transient maneuvers with non-negligible accelerations in all three dimensions.

$$\vec{a}(t) = a_x(t)\hat{i} + a_y(t)\hat{j} + (a_z(t) + g)\hat{k} \tag{1}$$

$$\hat{n}_a(t) = \frac{\vec{a}(t)}{|\vec{a}(t)|} \tag{2}$$

$$sin\gamma_{eff} = \frac{\vec{v} \cdot \hat{n}_a}{V} \tag{3}$$

Examples of the extracted and calculated vehicle state data for condition M1, fast cyclic right turn (NASA run number 206542), and condition M5, cyclic pitch-up (NASA run number 206550), are shown in Figures 2 and 4, respectively. The vehicle data from the M1 condition, shown in Figure 2, demonstrates the single-input nature of the maneuvers. Specifically, the vehicle was at a roll angle of nearly 75° at t = 0 s, meanwhile the pitch angle at that time was less than -5°, as opposed to a positive pitch angle to maintain altitude. The linear trend of the vehicle heading during the roll maneuver indicates that, although the entry into the roll reached 60°/s, the roll maneuver was executed as a smooth and consistent arc. A subset of additional vehicle information for run 206542 (M1), also highlighting the unsteadiness of the maneuvers, is shown in Figure 3, where the gray curves are from a steady, level flight at the same forward speed and entry altitude. The main rotor RPM deviated by less than ±0.3% during the steady level flight (± ≈1.5 RPM), whereas the RPM during the unsteady maneuver varied by over 11 RPM, which was ≈3%, an order of magnitude greater than the steady flight. The rate of change of the main rotor RPM (converted to radians per second squared in the figure) appears even more drastic, with the main rotor RPM varying rapidly throughout the maneuver. The engine output also greatly increased during the maneuver, to over double the torque required for the level flight. Similarly, during the M5 pitch-up maneuver, the heading remained almost unchanged and the roll angle was below 10° at t = 0 s while the vehicle was pitched up to almost 45°. Both of the test runs shown include strong decelerations in the X direction, ≈1 g, which is another clear indicator of the pilot's discipline in executing these as single-input maneuvers.

Acoustic Data

Synchronized collection of acoustic and vehicle state data allowed for the implementation of time-domain de-Dopplerization using the method described in Ref. 15. This method also allows for projection of the pressure time history to a virtual observer located on a sphere that travels with the vehicle, where the location of each microphone relative to the vehicle is then represented by azimuth (ψ) and elevation (θ) angles. All acoustic data shown in this work have been de-Dopplerized, distance-corrected onto a sphere with a radius of 30.48 m (100 ft), and will be shown as a function of source time. Atmospheric absorption has been neglected, given the

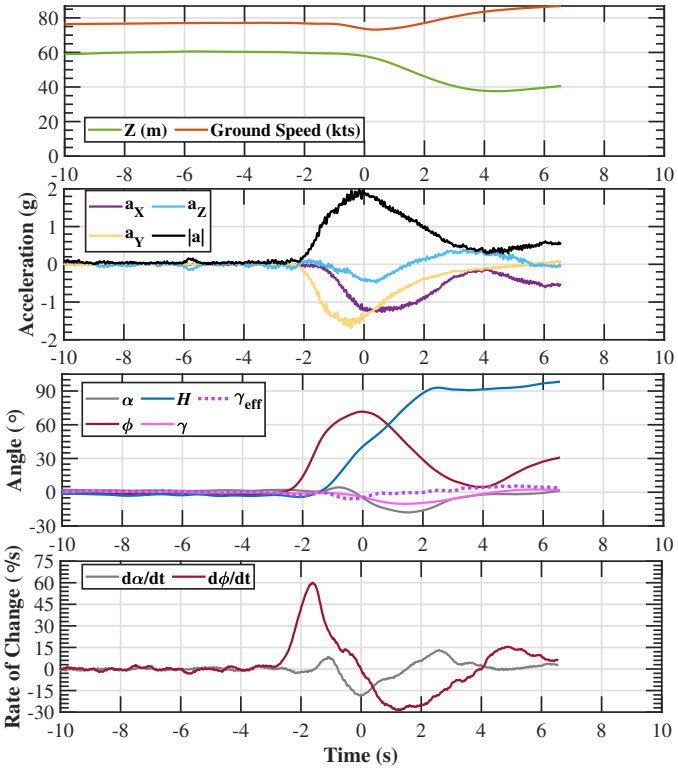

Figure 2: Vehicle state data for a cyclic roll right, Condition M1.

short propagation distances (typically ¡500 ft) and frequency range of interest. The de-Dopplerized pressure time histories were passed through a 10 Hz high-pass filter and then OASPL was calculated over 0.25-second intervals.

Unsteady maneuvers have traditionally been associated with the presence of blade-vortex interaction (BVI) (Refs. 16–18). The tail rotor for the MD530F is also known to be particularly noisy across frequencies shared with BVI noise. As such, BVI noise was extracted using the wavelet transform method described in Ref. 19, with the minimum frequency and amplitude cutoffs set to 6 BPF for the main rotor and -6 dB from the energy of the main rotor BPF, respectively. This method extracts the pressure time history data associated with BVI. Blade-vortex interaction sound pressure level (BVISPL) was then calculated using the BVI extracted pressure time histories, also over 0.25-second intervals. Pressure time histories provided in this work have been normalized such that a value of 1 is equal to the peak pressure across the array during the reference steady level flight at 75 kts. OASPL and BVISPL values will be shown in ΔdB, where 0 dB is the peak OASPL or BVISPL across the array during the reference condition. A sample comparison of OASPL and BVISPL from the point of peak roll angle for NASA run number 206542 is shown in Figure 5, where the gray circles are the microphone positions, the blue line is the flight track, the red dot is the vehicle location, and the black dashed curves represent ΔdB = 0. Note that

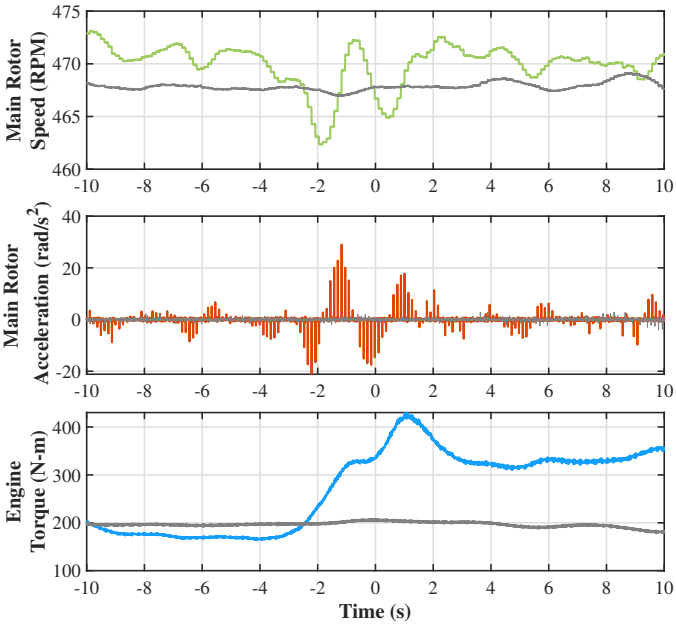

Figure 3: Example of measured unsteady vehicle data during a M1 cyclic roll right maneuver (colors) and a level flight (gray).

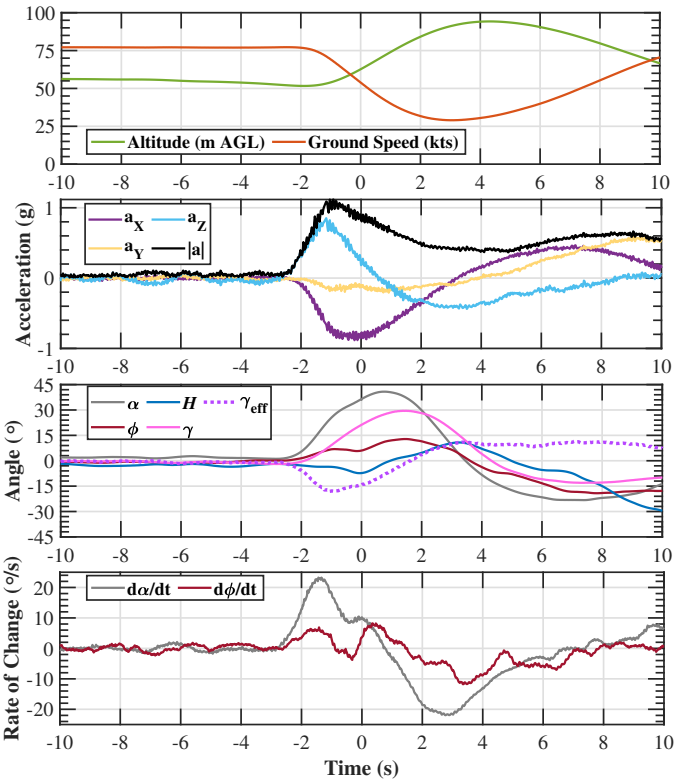

Figure 4: Vehicle state data for a cyclic pitch up, Condition M5.

the OASPL and BVISPL were calculated using pressure time histories that were de-Dopplerized and distance-corrected to a 30.48 m sphere, however, they are shown in the figure pro-

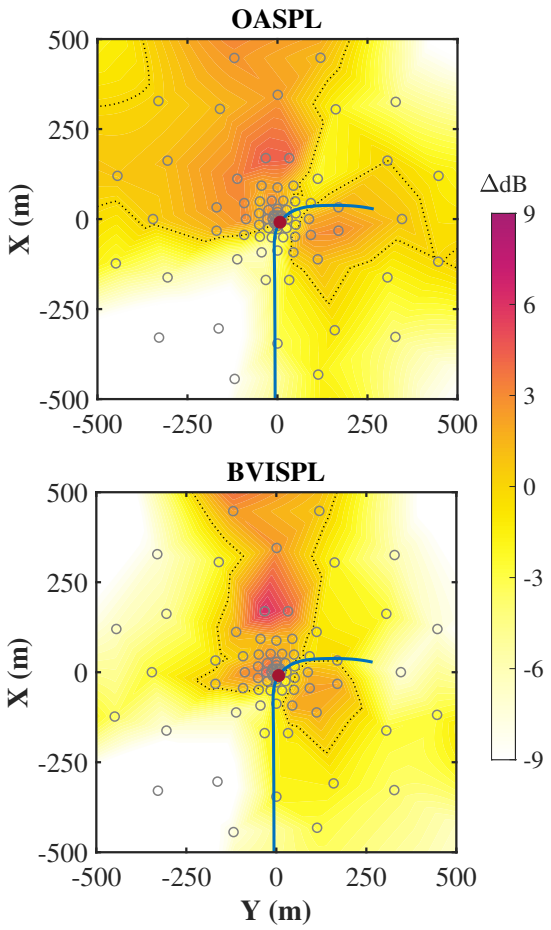

Figure 5: Comparison of OASPL and wavelet transform-extracted BVISPL for condition M1.

jected onto the ground plane. This is due to the nature of the maneuvers, where large pitch and roll motions result in some of the microphones being above the rotor plane and not located on a traditional lower hemisphere.

RESULTS AND DISCUSSION

This work will primarily focus on results from the more aggressive maneuver conditions from Table 1. These maneuvers provide a unique opportunity to investigate the acoustic emissions from highly atypical conditions, such as maximum roll angles of 60° to 75°, maximum roll rates approaching 60°/s, maximum pitch angles of almost 45°, and accelerations nearing 2 *g*.

Snapshot Array for Maneuvers

A snapshot array was deployed for this test, as opposed to a more traditional linear array. Linear microphone arrays typically operate on the principal that the vehicle is flying a steady condition such that a full hemisphere under the vehicle can be created by the different azimuthal and elevation angles that each microphone passes through during the flyover. The intent behind the snapshot array was to deploy the microphones in such a way that the entire hemisphere could be generated from one "snapshot" in time. This is anticipated to be important for UAM and FVL vehicles with distributed propulsion systems, where vehicle conditions such as propulsor rotation rate may not be reliably steady even in steady flight conditions. More details on the design of the array and analysis of its general performance are included in Ref. 10. An example of the microphone coverage at select points in time from an L3 steady, level flight is provided in Figure 6. The coverage is shown in a Lambert projection using the previously described convention. The projections are shown in chronological order, from left to right, corresponding with the times indicated by the dashed black lines. Times before and after the vehicle crosses over the center of the array are included to demonstrate the clustering and stretching effect that the vehicle approach and retreat from the array has on the position of the microphones relative to the vehicle. The center projection, at t = 0 s, is close to representative of the designed coverage condition of the array. The same five microphones with unique markers from Figure 1 are also marked in Figures 6 and 7.

A similar set of projections were also created for an M1 flight condition and are provided in Figure 7. The first and last selected times provide a reference for comparison with the L3 flyover shown in Figure 6. The remainder of the times highlight a large roll angle with little heading change (t = -1.5 s), the maximum roll angle (t = 0 s), and the peak pitch angle (t = 1.5 s). An additional Lambert projection covering the upper hemisphere around the vehicle (above the main rotor plane) has been added for each selected point, where the same convention is utilized for the azimuthal angles, and the elevation angles from 0° to 90° indicate the horizon to directly above the vehicle, respectively. The aggressive pitch and roll angles throughout these maneuvers highlight the limitations of ground-based microphone arrays, with the global horizon line almost cutting the upper and lower hemispheres in half at t = 0 s. However, the spherical coverage maintained throughout the maneuvers is still sufficient to allow for a significantly more comprehensive picture of the acoustic emissions than a linear array would be capable of. Note how the general axial symmetry of the array leads to the projections at t = 4 s in Figures 6 and 7 to be almost indistinguishable, if not for the specially marked microphones, even though the vehicle has made a 90° change in heading. The main limitation of the snapshot array is due to the microphones all being on the ground plane, limiting the range of elevation angles that can be captured at any given time. This restriction is likely to not have a simple solution, since past work has indicated that, even at altitudes as high as 305 m (1,000 ft), data from elevated microphones are corrupted by ground reflections (Ref. 20). Additionally, future UAM and FVL deployments are likely to be more concerned with unsteadiness in the vehicle state than with aggressive ma-

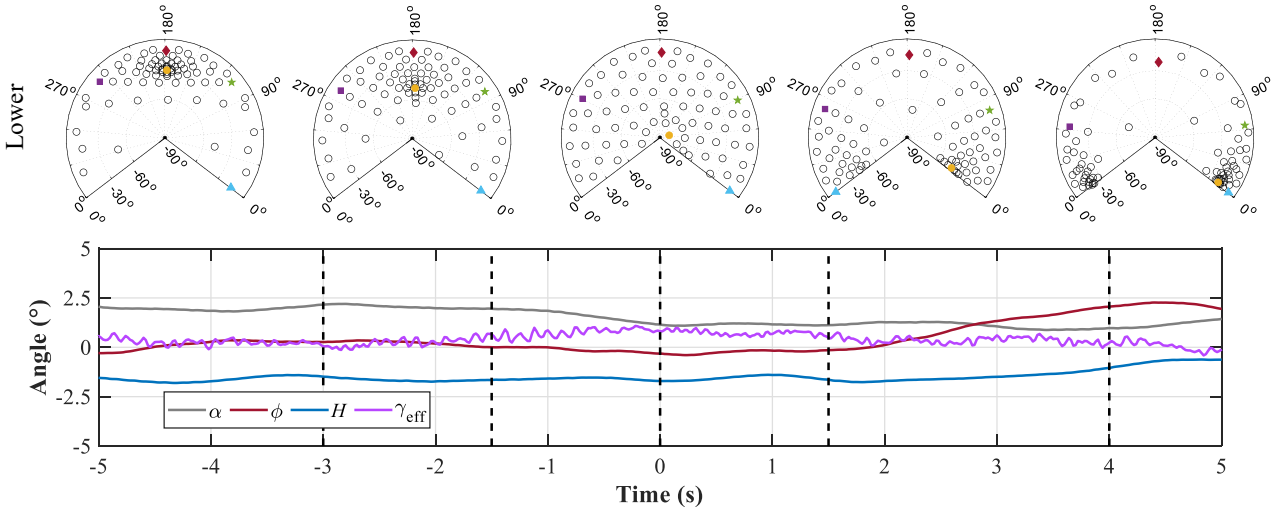

Figure 6: Lambert projections of microphone distributions at selected times for condition L3.

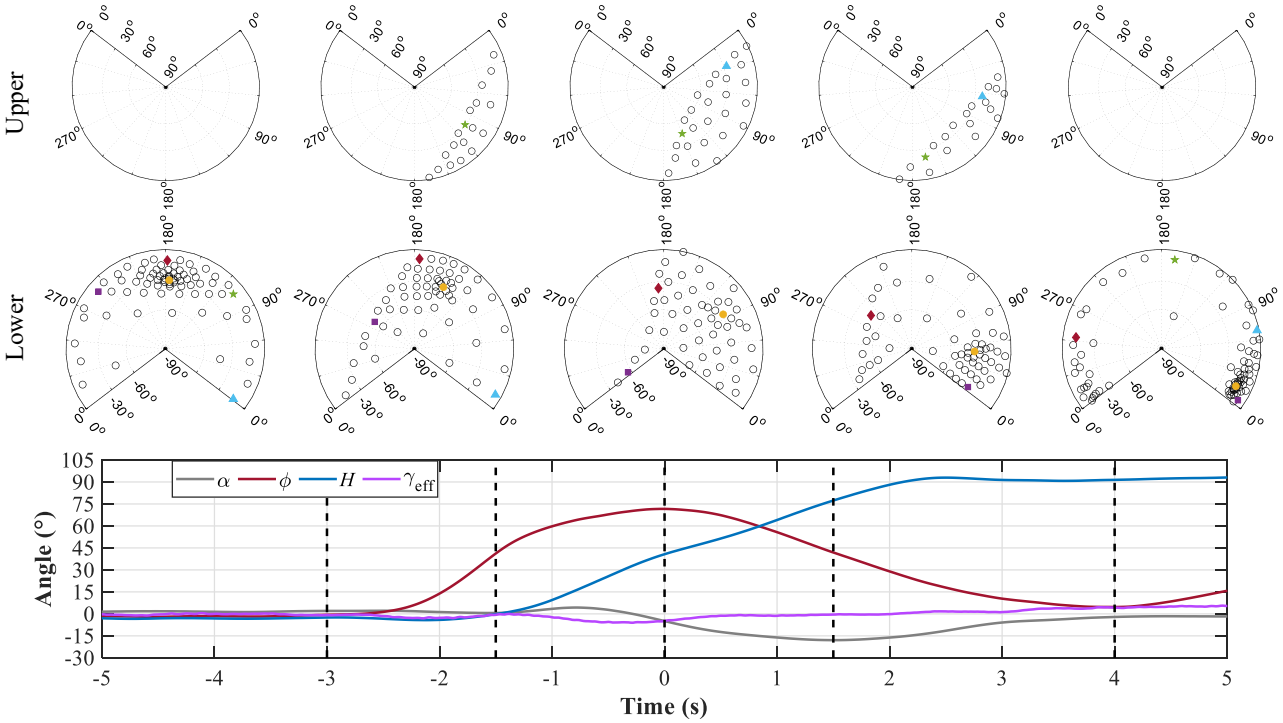

Figure 7: Lambert projections of microphone distributions at selected times for condition M1.

neuvers like the ones performed in this test.

Pitching Maneuvers

The pitching conditions will first be considered. Review of the vehicle state data for the pitch-up maneuvers indicated that the cyclic pitch-up maneuvers (M5) were significantly more aggressive than the collective pitch-up maneuvers (M6) in terms of maximum pitch angle, maximum pitch rate, and acceleration. This is not surprising given the mechanics of helicopter controls. It is therefore also not surprising that the combined cyclic and collective pitch-up maneuvers (M7) were dominated by the cyclic control input and the vehicle state data and acoustic emissions from these runs very closely matched those from condition M5. A subset of this data is provided in Figure 8, where the legend is shown in order of increasing NASA combined run number from 206550 to 206555. An interesting observation across all of the pitch-up cases is the

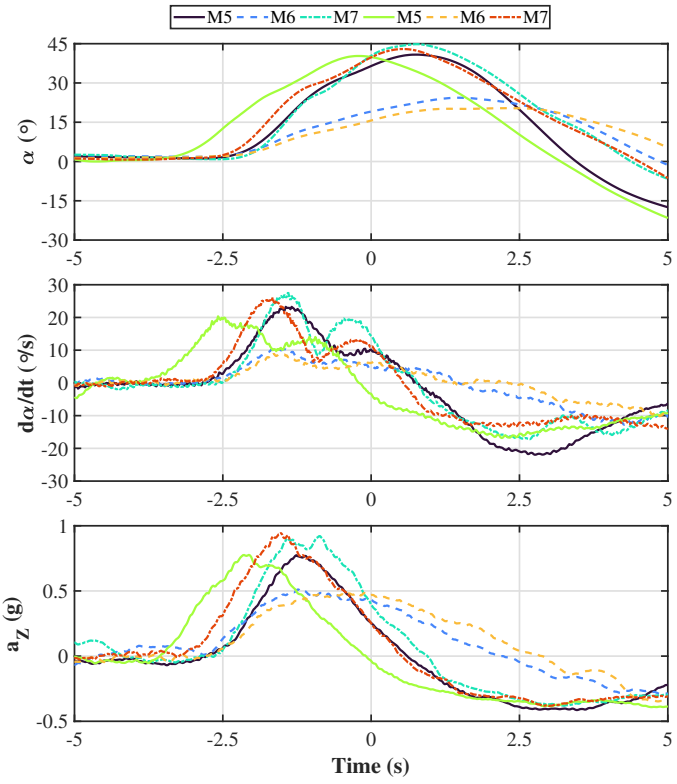

Figure 8: Subset of vehicle state data vs. time for pitch-up maneuvers.

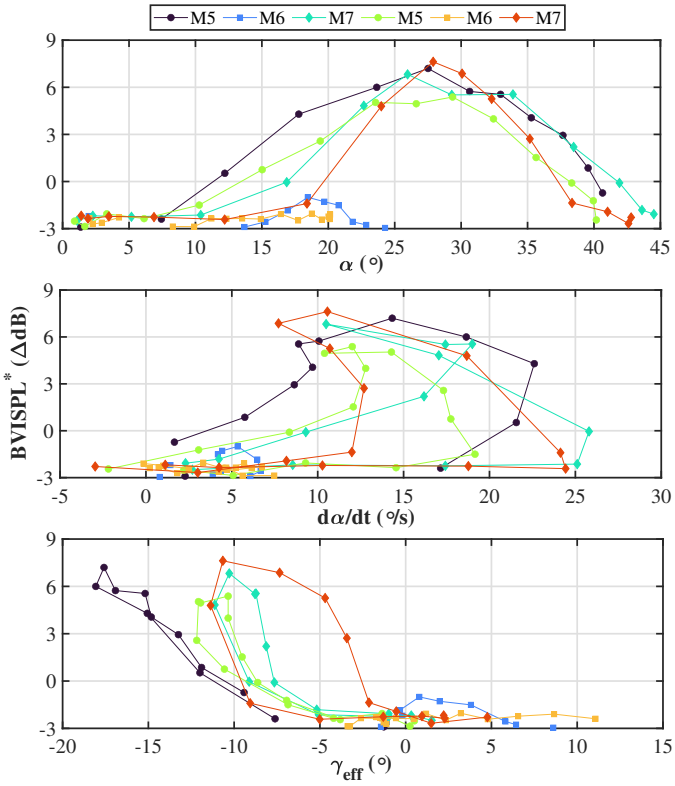

Figure 9: Subset of vehicle state data and BVISPL for pitch-up maneuvers.

double-hump in pitch rate. Given that the pitch angle and vertical acceleration remained fairly steady, it is possible that this was due to the vehicle passing through a thermal updraft. The maneuvers were all flown during the second sortie of flight day 206, when the temperature was increasing. The majority of the test area that the vehicle flew over was a loose, dry dirt, however a compacted gravel pad was near the center of the array, and the pilot reported thermal updrafts during the sortie, all suggesting thermals to be the culprit.

Acoustic data were then analyzed against the vehicle state data to investigate possible contributions to the noise generation. Acoustic emissions as a function of vehicle state are provided for a subset of relevant state variables in Figure 9. Note that the data in Figure 9 are shown as BVISPL*, where BVISPL* is the mean value across the array of all BVISPL $\geq -3\Delta$dB. The general trend in BVISPL* agree with the previous observations that the collective pitch-up maneuvers (M6) were significantly less aggressive than the cyclic (M5) or cyclic-collective combination (M7) pitch-up maneuvers, and that there is good agreement between the M5 and M7 maneuvers. An initial takeaway from this data is that the BVISPL* during the collective pitch-up maneuver never exceeded that of the L3 flyover, suggesting that it is generally the more acoustic-conscious maneuver. The BVISPL* data, when plotted against multiple state parameters, indicates that the strong acoustic emissions during the more aggressive pitch-up maneuvers are driven primarily by the acceleration of vehicle. The plots in Figure 9 show that the BVISPL* did not occur at the peak pitch angle or pitch rate, but instead the hysteresis arc in the bottom plot shows that it did occur at the point of peak γ_{eff}. Recall that γ_{eff} is the effective flight path angle when taking three-dimensional accelerations into account.

Extracted BVI pressure time histories for a cyclic pitch up (M5) maneuver were queried to further investigate the relationship between BVI noise and pitch angle, pitch rate, and γ_{eff}. Specifically, this was NASA combined run number 206550, which was also presented in Figure 4. The microphone with the highest BVISPL at peak pitch angle was identified along with microphones at similar azimuth and elevation angles at the times of peak pitch rate and γ_{eff}. This was done to provide a more one-to-one comparison while simultaneously helping to identify the directivity of the BVI noise. The plots in Figure 10 are organized chronologically, such that the top plot occurred first, and the dashed lines show the location in time each peak value. The extracted pressure time histories show that almost no BVI content was present at the maximum pitch angle, and that the strength of the BVI impulses during the time of peak γ_{eff} were approximately double those during the peak pitch rate. The azimuth and elevation angles in Figure 10 also show that the peak BVI directivity was ahead of the vehicle slightly to the advancing side and roughly 60° below the horizon, which is consistent with expected BVI

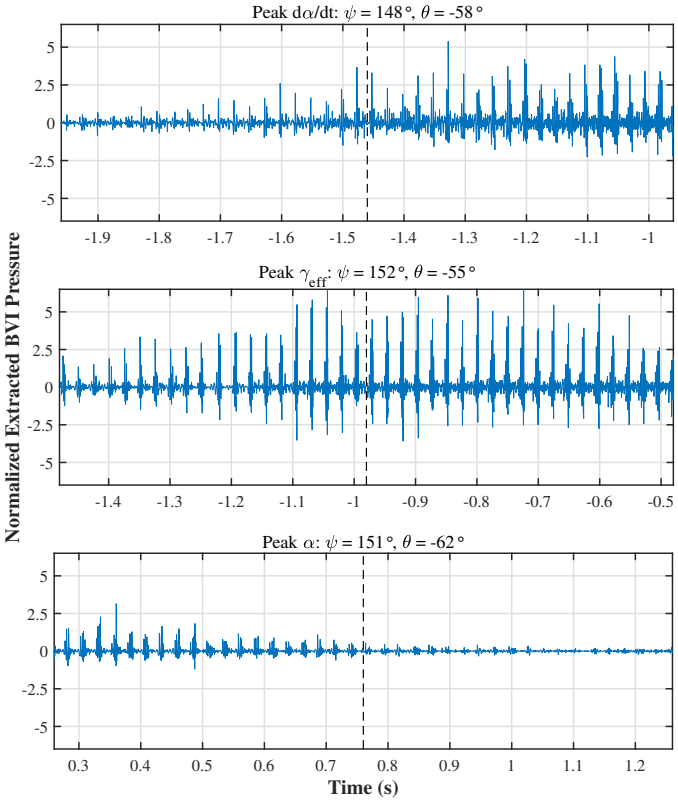

Figure 10: Wavelet transform-extracted pressure time histories for condition M5.

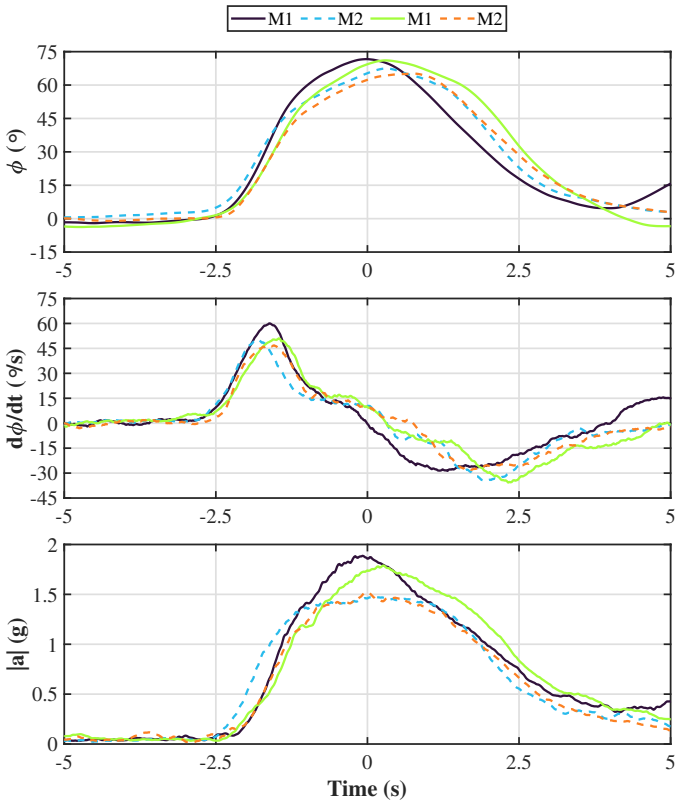

Figure 11: Subset of vehicle state data vs. time for rolling maneuvers.

directivity. These results, taken together with those in Figures 4 and 9, suggest that the BVI noise generated during the pitch-up maneuvers were due to rapid longitudinal deceleration and vertical acceleration (both close to 1 g), combined with a pitching up of the rotor plane, causing the forward portion of the main rotor to interact with its own wake. However, this would likely require a portion of the wake near the nose of the vehicle to be above the rotor plane during steady level flight. An alternative possibility is that the same factors led to the aft portion of the main rotor to pitch down into the wake. More advanced modeling of the rotor wake is required to determine the validity of these hypotheses.

Rolling Maneuvers

Transient rolling maneuvers are often considered favorable conditions for the generation of BVI noise (Refs. 14,21). Only the "fast" rolling maneuvers will be investigated in this work, the cyclic roll right (M1) and cyclic roll left (M2). Key aspects of the vehicle state during these maneuvers are compared in Figure 11, where the legend entries are in order based on NASA combined run numbers from 206542 to 206545. Importantly, the general conditions experienced by the vehicle during the left and right rolls were very similar (note that the negative of roll angle and roll rate are shown for the left turns to aid in the comparison). The largest deviation between the M1 and M2 conditions were in the accelerations, with the vehicle experiencing roughly 25% less total acceleration during the M2 maneuvers. All three components of acceleration were lower for the M2 maneuvers, with the largest discrepancy (roughly 20%) in the Y direction (normal to the primary flight path). However, it is important to note that although the differences in acceleration between the two maneuvers is non-negligible, the maximum acceleration for the "weaker" rolls was still near 1.5 g, making these very aggressive maneuvers. The similarity in vehicle state data between the M1 and M2 conditions creates a valuable opportunity for comparison. In addition, it isolates the differences between the two maneuvers almost exclusively to the effects of the relative rotation direction of the rotors.

Acceleration appeared to be the largest driver of BVI noise generation in the pitch-up maneuvers; however, BVI in rolling maneuvers is generally considered to be determined more by roll direction. The main rotor for the MD530F rotates counter-clockwise, so rolls towards starboard (M1) are towards the advancing side of the main rotor and rolls towards port (M2) to the retreating side. The expectation is that rolling towards the advancing side of the main rotor are more prone to strong BVI (Ref. 22). With that expectation in mind, the BVISPL values across the microphone array during M1 and M2 maneuvers are compared in Figure 12. Both plots are taken from

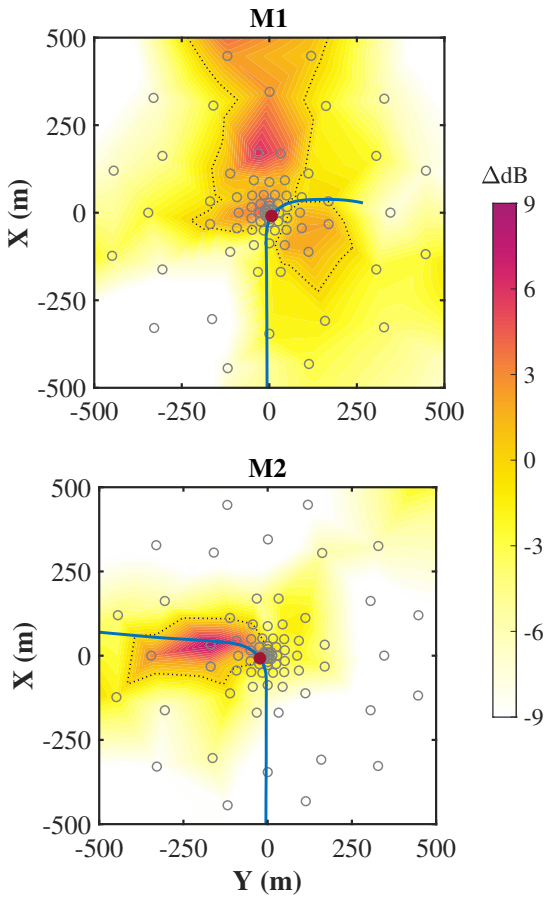

Figure 12: Comparison of BVISPL for conditions M1 and M2.

the point of maximum roll angle, which was also the point with the strongest BVISPL for both cases. Immediately, the strength and distribution of the BVISPL in each maneuver draws attention. The relative strength of the BVISPL for both maneuvers is similar; however, the projected area and directivity are significantly different.

BVI pressure time histories for the rolling maneuvers were extracted in a similar manner as the pitching maneuvers (i.e. from times around the points of peak roll angle, roll rate, and γ_{eff}) to investigate the contributions to the BVI noise. First, Figure 13 shows the pressure time histories for the M1 maneuver. Strong BVI impulses appear to occur at the maximum roll angle, directed towards the nose of the vehicle, with significantly lower impulse amplitudes correlating to the periods of peak roll rate and γ_{eff}. The alignment of strong BVI with the peak roll angle appears somewhat at odds with the alignment with peak γ_{eff} and not peak pitch angle for the pitch-up maneuver. However, Figure 14 provides valuable insight into why these observations are actually aligned. During the pitch-up maneuvers, the vehicle is actively fighting gravity, causing the parabolic trend in pitch angle vs acceleration and leading to the maximum acceleration aligning in time with the peak

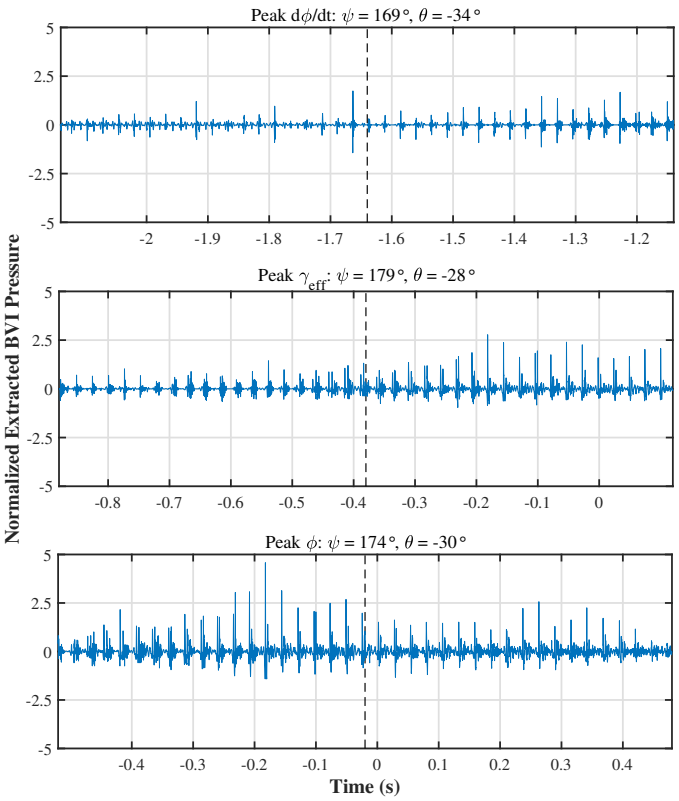

Figure 13: Wavelet transform-extracted pressure time histories for condition M1.

γ_{eff} and not the peak pitch angle. Conversely, since the maneuvers were executed as approximately single-input maneuvers, the vehicle rapidly lost altitude during the roll maneuvers, allowing roll angle to have a linear relationship with acceleration and leading to the maximum acceleration and roll angle aligning in time. Interestingly, although the peak γ_{eff} occurs at the point of peak acceleration for the pitch-up maneuvers, Figure 14 shows that peak γ_{eff} occurs before the peak acceleration for the rolling maneuvers. Taken together, the results from the M1 and M5 maneuvers indicate that the best predictor of when the BVI noise will be strongest during aggressive maneuvers is the acceleration of the vehicle.

The question still remains as to why the BVI noise during the retreating-side maneuver appears as strong as it does. Extracted pressure time histories for the M2 maneuver are shown in Figure 15. The strong impulses are observed near the peak roll angle, similar to the M1 roll, which was also shown in Figure 14 to be near the maximum acceleration for these maneuvers. It is possible for retreating-side roll maneuvers to lead to BVI. However, the directivity of the noise from the M2 maneuver is ahead and to port near the horizon, whereas retreating-side BVI noise is expected to radiate behind the vehicle (Ref. 23). Another interesting observation is in the period of the BVI impulses. The period of the main rotor BPF is 0.0252 s, meaning there should be approximately 4 impulses in between each x-axis tick mark in the pressure time history

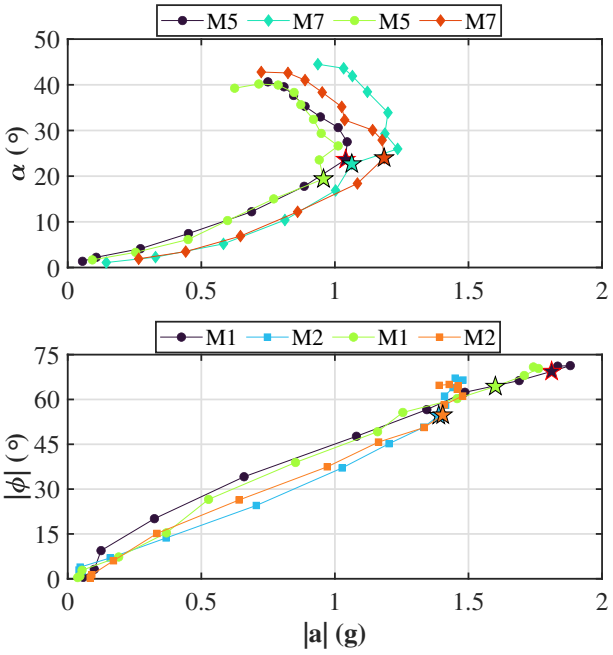

Figure 14: Comparison of pitch (top) and roll (bottom) angles vs acceleration where the stars indicate the point of peak γ_{eff}.

figures. This is true for the impulses shown in Figures 10 and 13, however there appear to be 9 to 10 impulses between tick marks in Figure 15. Consequently, the tail rotor BPF was 94.9 Hz, leading to a period of 0.0105 s and an expectation of observing roughly 10 impulses between tick marks. Recall that the wavelet transform was performed on the data such that all frequency content below 6 BPF, based on the main rotor BPF, was removed. The minimum frequency cutoff would remove the tail rotor BPF and second harmonic, relying on the amplitude, relative to the energy of the main rotor BPF, for the removal of higher order tail harmonics. Typically, this is assumed sufficient, however tail rotor BVI content could be retained if the energy in the tail rotor BVI noise was less than 6 dB below that of the main rotor BPF. This suggests that the BVI noise observed in the fast cyclic left rolls may actually be tail rotor BVI noise. A rotation into azimuth and elevation angles relative to the tail rotor plane would then locate the bottom pressure time history in Figure 15 to approximately ahead and below the tail rotor, which is a more standard direction for BVI noise. The directivity relative to the tail rotor frame indicates that the BVI is occurring between the tail rotor and its own wake, not the tail rotor and wake of the main rotor. The physics also would allow for this possibility, since a starboard roll (leading to a counter-clockwise yaw) would swing the tail boom into the wake of the tail rotor. A more rigorous method for extracting only the main rotor noise contributions, such as a Vold-Kalman filtering process, would be needed to definitively attribute the BVI noise during the M2 maneuvers to the tail rotor, however the current analysis strongly suggests that is the case.

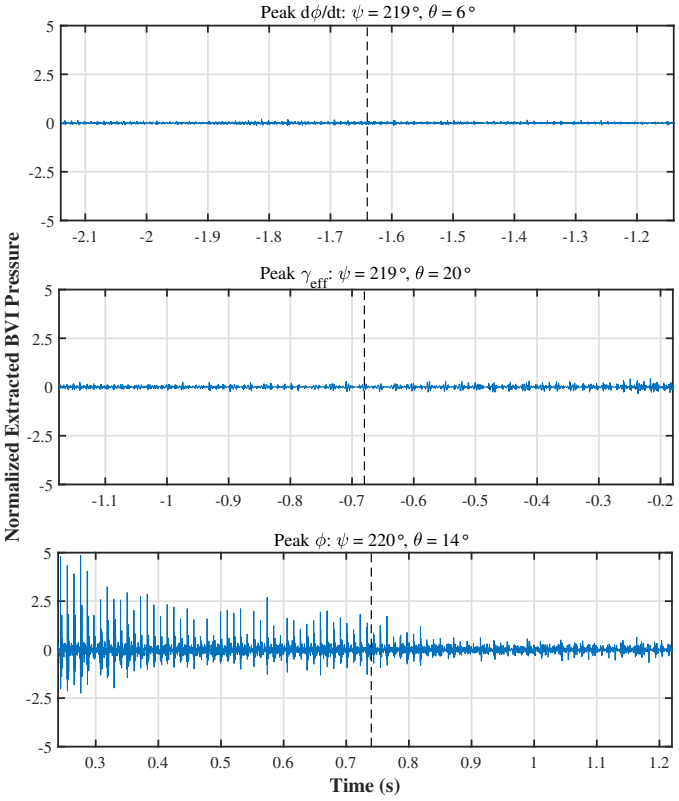

Figure 15: Wavelet transform-extracted pressure time histories for condition M2.

CONCLUSIONS

Data was collected for unsteady maneuvers during a recent Army/NASA joint flight test of an MD530F helicopter. These unsteady maneuvers were intended to provide an opportunity to apply experimental methods and analysis techniques to unsteady flight in preparation for future tests with UAM and FLV vehicles. A snapshot microphone array was deployed for the test, which was designed to provide full coverage of an acoustic hemisphere at a near-instant in time. This removed the reliance on the assumption of steadiness that is required when utilizing linear microphone arrays. An investigation of the microphone projections onto a vehicle-centered sphere demonstrated that, although limited by the microphones all being placed on the ground, the array design was well-suited to capturing unsteady flight conditions. Analysis of the acoustic emissions during the maneuvers indicated the presence of BVI noise. This was expected for the conditions where the vehicle rolled towards the advancing side of the main rotor; however, BVI noise was also present in the rolls towards the retreating side of the main rotor and during pitch-up maneuvers. Further investigation into the retreating-side roll suggests that the BVI noise captured was actually generated by the tail rotor. It was hypothesized that BVI during the pitch-up maneuver required some portion of the main rotor wake be above the main rotor during steady, level flight, but modeling of the rotor wake will

likely be required to determine if that is the cause. A commonality across the BVI-generating maneuvers was that the maximum strength of the maneuver occurred near the point of maximum vehicle acceleration. Interestingly, this aligned closer with the peak pitch rate during the pitch up maneuvers and the peak roll angle during the rolling maneuvers. This was determined to be a result of the single-input nature of the maneuvers, which allowed the vehicle to maintain an increase in acceleration during the rolling maneuvers but not the pitch-up maneuvers.

ACKNOWLEDGMENTS

The authors would like to sincerely thank Dr. Eric Greenwood for his helpful discussion on maneuvering physics and suggestion to investigate applicability of effective flight path angle. Funding for this work was provided by the U. S. Army Combat Capabilities Development Command Aviation & Missile Center and the NASA Revolutionary Vertical Lift Technology project.

REFERENCES

1. Greenwood, E., Brentner, K. S., Rau, R. F., and Ted Gan, Z. F., "Challenges and Opportunities for Low Noise Electric Aircraft," *International Journal of Aeroacoustics*, Vol. 21, (5-7), 2022, pp. 315–381. doi: 10.1177/1475472X221107377

2. Pascioni, K. A., Thai, A. D., and Bain, J. J., "Propeller Source Noise Separation from Flight Test Measurements of the Joby Aviation Aircraft," 30th AIAA/CEAS Aeroacoustics Conference (2024), AIAA 2024-3231. doi: 10.2514/6.2024-3231

3. Gan, Z. F., Mukherjee, B., Theron, J.-P., Botre, M., Brentner, K. S., Greenwood, E., and Horn, J. F., "A New Distributed Electric Propulsion Aircraft Simulation Tool for Coupled Flight Dynamics, Free Wake, and Acoustic Predictions," Proceedings of the 77^{th} Annual Forum of the Vertical Flight Society, Virtual, May 2021. doi: 10.4050/F-0077-2021-16693

4. Mukherjee, B., Jue, A., Theron, J.-P., Brentner, K. S., Greenwood, E., and Horn, J. F., "Investigation of Departure Transition Noise for Lift-Plus-Cruise eVTOL Aircraft," Proceedings of the 79^{th} Annual Forum of the Vertical Flight Society, West Palm Beach, FL, May 2023. doi: 10.4050/F-0079-2023-17938

5. Schmitz, F. H., Greenwood, E., Sickenberger, R. D., Gopalan, G., Sim, B. W.-C., Conner, D., III, E. M., and Decker, W. A., "Measurement and Characterization of Helicopter Noise in Steady-State and Maneuvering Flight," Proceedings of the 63^{rd} Annual Forum of the Vertical Flight Society, Virginia Beach, VA, May 2007.

6. Spiegel, P., Guntzer, F., Duc, A. L., and Bucholz, H., "Aeroacoustic Flight Test Data Analysis and Guidelines for Noise Abatement-Procedure Design and Piloting," Proceedings of the 65^{th} Annual Forum of the Vertical Flight Society, Grapevine, TX, May 2009.

7. Watts, M. E., Snider, R., Greenwood, E., and Baden, J., "Maneuver Acoustic Flight Test of the Bell 430 Helicopter," Proceedings of the 68^{th} Annual Forum of the Vertical Flight Society, Fort Worth, TX, May 2012.

8. Watts, M. E., Greenwood, E., Smith, C. D., Snider, R., and Conner, D. A., "Maneuver Acoustic Flight Test of the Bell 430 Helicopter Data Report," Technical Memorandum NASA/TM-2014-218266, NASA Langley Research Center, Hampton, VA 23681, USA, May 2014.

9. Stephenson, J. H., Pascioni, K. A., Houston, M. L., Stutz, C. M., and Martin, P. B., "Overview of a Comprehensive MD530F Acoustic Flight Test," Proceedings of the 81^{st} Annual Forum of the Vertical Flight Society, Virginia Beach, VA, May 2025.

10. Houston, M. L., Stephenson, J. H., Stutz, C. M., and Pascioni, K. A., "Snapshot Array Design Considerations for Rotorcraft Noise Characterization," Proceedings of the 81^{st} Annual Forum of the Vertical Flight Society, Virginia Beach, VA, May 2025.

11. Stephenson, J. H. and Pascioni, K. A., "Design of Experiments Development for Rotorcraft Acoustic Flight Testing," Proceedings of the 81^{st} Annual Forum of the Vertical Flight Society, Virginia Beach, VA, May 2025.

12. Pascioni, K. A., Greenwood, E., Watts, M. E., Smith, C. D., and Stephenson, J. H., "Medium-Sized Helicopter Noise Abatement Flight Test Data Report," Technical Memorandum NASA/TM-2014-218266, NASA Langley Research Center, Hampton, VA 23681, USA, May 2020.

13. Stephenson, J. H., Lind, A., Hutchins, C., Pascioni, K., Houston, M. L., and Martin, P., "Yuma 2022 Rotorcraft Acoustic Flight Test," Technical Memorandum NASA/TM-20220004483, NASA Langley Research Center, Hampton, VA 23681, USA, April 2022.

14. Greenwood, E. and Rau, R., "A Maneuvering Flight Noise Model for Helicopter Mission Planning," *Journal of the American Helicopter Society*, Vol. 65, (2), 2020, pp. 022007. doi: 10.4050/JAHS.65.022007

15. Greenwood, E. and Schmitz, F. H., "Separation of Main and Tail Rotor Noise from Ground-Based Acoustic Measurements," *Journal of Aircraft*, Vol. 51, (2), March 2014, pp. 464–472. doi: 10.2514/1.C032046

16. Schmitz, F. H., Greenwood, E., Sickenberger, R. D., Gopalan, G., Sim, B. W.-C., Conner, D., Moralez, E., and Decker, W. A., "Measurement and Characterization of Helicopter Noise in Steady-State and Maneuvering Flight," Proceedings of the 63^{rd} Annual Forum of the American Helicopter Society, Virginia Beach, VA, May 2007.

17. Sickenberger, R., Gopalan, G., and Schmitz, F. H., "Helicopter Near-Horizon Harmonic Noise Radiation due to Cyclic Pitch Transient Control," Proceedings of the 67^{th} Annual Forum of the American Helicopter Society, Virginia Beach, VA, May 2011.

18. Stephenson, J. H., Tinney, C. E., Greenwood, E., and Watts, M. E., "Time Frequency Analysis of Sound from a Maneuvering Rotorcraft," *Journal of Sound and Vibration*, Vol. 333, (21), 2014, pp. 5324–5339.
doi: 10.1016/j.jsv.2014.05.018

19. Stephenson, J. H. and Tinney, C. E., "Extracting Blade-Vortex Interactions Using Continuous Wavelet Transforms," *Journal of the American Helicopter Society*, Vol. 62, (2), 2017, pp. 1–10.
doi: 10.4050/JAHS.62.022001

20. Sickenberger, R., Schmitz, F., and Jaeger, S. M., "Rotorcraft External Far-Field Noist Measurement Using a Hot Air Balloon," Proceedings of the 74^{th} Annual Forum of the Vertical Flight Society, Phoenix, Az, May 2018.
doi: 10.4050/F-0074-2018-12668

21. Chen, H.-n., Brentner, K. S., Ananthan, S., and Leishman, G. J., "A Computational Study of Helicopter Rotor Wakes and Noise Generated During Transient Maneuvers," *Journal of the American Helicopter Society*, Vol. 53, (1), 2008, pp. 37–55.
doi: 10.4050/JAHS.53.37

22. Stephenson, J. H., Watts, M. E., Greenwood, E., and Pascioni, K. A., "Development and Validation of Generic Maneuvering Flight Noise Abatement Guidance for Helicopters," *Journal of the American Helicopter Society*, Vol. 67, (1), January 2022, pp. 1–12.

23. Schmitz, F. H. and Sim, B. W.-C., "Radiation and Directionality Characteristics of Helicopter Blade-Vortex Interaction Noise," *Journal of the American Helicopter Society*, Vol. 48, (4), 2003, pp. 253–269.
doi: 10.4050/JAHS.48.253